Monthly Notices of the ROYAL ASTRONOMICAL SOCIETY

MNRAS **539**, 1955–1963 (2025)
Advance Access publication 2025 April 15

https://doi.org/10.1093/mnras/staf614

Laser guide stars as comparison stars: correcting scintillation noise

Kathryn E. Hartley [1]★ Domenico Bonaccini Calia [1] Felipe Pedreros Bustos,[2] Mauro Centrone,[3] David Jenkins,[4] Richard W. Wilson [1] and James Osborn [1]

[1] Centre for Advanced Instrumentation, Department of Physics, University of Durham, South Road, Durham DH1 3LE, UK
[2] European Southern Observatory, Karl-Schwarzschild-Straße 2, D-85748 Garching bei München, Germany
[3] INAF Osservatorio Astronomico di Roma, Via Frascati 33, I-00078 Monte Porzio Catone, RM, Italy
[4] European Space Agency-ESA/ESTEC, CSC-SQ, Keplerlaan 1, NL-2201 AZ Noordwijk, the Netherlands

Accepted 2025 April 3. Received 2025 April 3; in original form 2024 October 21

ABSTRACT

The Earth's atmosphere severely limits ground-based high precision photometry. Whilst adaptive optics can be used to improve image resolution, intensity fluctuations due to scintillation and atmospheric transparency variations remain. Scintillation noise cannot typically be corrected with a comparison star as it is produced by high altitude turbulence, and therefore the range of angles over which it is correlated is very small. Comparison stars can be used to correct for atmospheric transparency variations, however, its shot noise, as well as differences in the airmass along the lines of sight for each star, add noise to the calibration. These noise sources significantly limits ground-based observations of time-varying astronomical sources such as exoplanet transits. We propose a new technique to correct for these effects by superimposing a sodium laser guide star (LGS) with a science target star, therefore creating an artificial photometric reference beacon that passes along the same line of sight. The measured LGS photometry can then be used to correct the intensity variations of the target star due to scintillation. Simulation results exploring this proposed technique are presented along with results from an on-sky test of this experiment conducted in La Palma, Spain, using a simple instrument to image the LGS and the target star light sources separately onto a single detector. On-sky tests were able to reduce the variance of the light curve for the target star on average by a factor of 2.8 ± 0.6. This demonstrates the technique and we expect that higher correction could be achieved.

Key words: instrumentation: miscellaneous – methods: observational – techniques: photometric – telescopes.

1 INTRODUCTION

High-precision ground-based time-resolved photometry is vital for a range of studies that look for small intrinsic variations in the intensity of astronomical sources. For example, for exoplanet photometry follow-up observations are needed in order to verify the transit detection, to check for variations in the transit timings, and to improve the precision on transit parameters such as the period and depth (Collins et al. 2018). However, such observations can be significantly limited by the effects of the Earth's atmosphere (Föhring et al. 2019) (Pont, Zucker & Queloz 2006).

As the light from an astronomical source passes through the atmosphere, high altitude regions of optical turbulence induce wave-front aberrations, which then propagate to produce spatial intensity fluctuations across the telescope pupil known as scintillation patterns. These spatial intensity patterns change over time as the turbulence evolves and translates with the wind (Dravins et al. 1997). This results in photometric noise known as scintillation on the order of ~ 0.1 per cent to ~ 1 per cent (Osborn et al. 2015) averaged over exposures of a few seconds. For bright stars scintillation noise is the dominant noise source.

Since scintillation is an effect of propagation, it is mainly created by high altitude turbulence. As such, correcting scintillation noise is a significant challenge. Differential photometry cannot normally be used to correct scintillation noise since the angular correlation of the intensity fluctuations is very small (Kornilov 2012). The probability of there being a bright comparison star within this angle is small – on the order of a few arcseconds. Several scintillation correction techniques have been proposed including correction using a tomographic algorithm (Osborn 2014; Hartley et al. 2023). However, such techniques require large telescopes and a tomographic AO facility. Hence, they are not suitable for small telescopes where scintillation is more significant.

We propose a new technique to correct scintillation noise by using a laser guide star (LGS) as an artificial comparison star. The LGS launch telescope can be located a few metres from the astronomical telescope. The LGS beacon can then be superimposed with a target star such that the light from both sources pass along the same path. A narrow band dichroic beam splitter centred on the Sodium D line at 589.2 nm can be used to separate the two light signals. The LGS light curve can then be used to correct the scintillation intensity fluctuations of the target star light curve using differential photometry. A key benefit of this technique over other scintillation correction techniques is that it can be used for any size of telescope.

Another important benefit of this technique is that it simultaneously corrects for transparency variations. Atmospheric transparency

★ E-mail: Kathryn.e.hartley@durham.ac.uk

variations significantly limit ground-based exoplanet transit photometry (Pont et al. 2006) but they can be corrected using comparison stars. However, when using a natural comparison star, the shot noise of the comparison star, as well as any differences in the airmass along the lines of sight for each star, add noise to the calibration (Mann, Gaidos & Aldering 2011). The use of an LGS directly along the line of sight will mitigate both of these error sources, potentially leading to very high precision ground-based photometry.

In this paper we explore this proposed technique. We discuss several possible error sources such as the cone effect, LGS elongation and variations in the LGS return flux. In addition, we present the results from an on-sky experiment to test the technique using the ESO Wendelstein LGS Unit (Bonnacini Calia et al. 2012) at the Roque de los Muchachos Observatory, La Palma, Spain.

2 THEORY

2.1 Scintillation

Scintillation is a source of photometric noise produced by the propagation of starlight through optical turbulence in the atmosphere. Regions of differing refractive indices can either focus or de-focus the incoming stellar wavefront resulting in spatial intensity fluctuations at the ground known as scintillation patterns. These patterns then change over time both as the turbulence moves with the wind and as it evolves (Dravins et al. 1997).

Since scintillation is an effect of propagation, it is mainly caused by turbulence in the upper atmosphere. As such, it is possible to have good photometric conditions in bad seeing as the angular seeing results from the strongest turbulence layer which is often close to the ground (Osborn et al. 2010). In addition, the angle over which the scintillation is strongly correlated will be much smaller than the typical separation of bright stars (Kornilov 2012). Hence, comparison stars cannot ordinarily be used to correct for scintillation, as the probability of finding a bright star within this angle is very small.

In astronomical photometry, assuming that there are no other noise sources, scintillation is quantified by the scintillation index which is simply a measure of the variance of the normalized intensity fluctuations:

$$\sigma_I^2 = \frac{\langle I^2 \rangle - \langle I \rangle^2}{\langle I \rangle^2}, \tag{1}$$

where I is the intensity of the star and $\langle \cdot \rangle$ is the time average.

For bright stars, scintillation is the dominant noise source and it significantly limits ground-based time-resolved photometry such as the study of exoplanet transits (Föhring et al. 2019).

For short exposure times, and for telescopes with an aperture $D \gg r_f$, where r_f is the Fresnel radius, the scintillation index can be estimated as (Sasiela 2012):

$$\sigma_I^2 = 17.34 D^{-7/3} (\cos(\gamma))^{-3} \int_0^\infty h^2 C_n^2(h) \mathrm{d}h, \tag{2}$$

where D is the telescope aperture, γ is the zenith angle, h is the altitude of the turbulent layer, and $C_n^2(h)$ is the refractive index structure constant.

For long exposure times, such that $t \gg t_{\mathrm{cross}}$ where t_{cross} is the time taken for the layer to cross the telescope pupil, the scintillation index is estimated as (Sasiela 2012):

$$\sigma_I^2 = 10.66 D^{-4/3} t^{-1} (\cos(\gamma))^{\alpha} \int_0^\infty \frac{h^2 C_n^2}{V_\perp(h)} \mathrm{d}h, \tag{3}$$

where t is the exposure time and $V_\perp(h)$ is the wind velocity profile. The value of α depends on the wind direction and will be -3 when the wind is transverse to the azimuthal angle of the star and -4 when it is longitudinal.

Based on these equations, scintillation is therefore more significant for small telescope apertures. For short exposure times, the intensity speckles will appear frozen in the pupil, whereas for long exposure times the speckles will move across the pupil during the exposure, resulting in temporal averaging (Roddier 1981). The degree of temporal averaging will depend on the wind speed and the exposure time.

2.2 Atmospheric transparency variations

Atmospheric transparency variations due to changes in molecular absorption and scattering from molecules and aerosols in the atmosphere is a source of photometric noise that limits ground-based photometry (Zou et al. 2010) (Pont et al. 2006). These transparency variations have a power spectrum proportional to $1/f$ (Young et al. 1991), where f is the temporal frequency. The atmospheric transparency variations can vary significantly from night to night, as well as seasonally (Zou et al. 2010) making it very hard to estimate.

This noise source is often correlated over a much larger angle than scintillation noise and therefore can often be corrected using a comparison star. When properly applied, differential photometry techniques can obtain high accuracies with errors as low as ± 0.001 magnitude (Howell 2006). However, differential photometry is often limited by the magnitude of the comparison star as the noise from the two stars will add in quadrature. Therefore, the ideal comparison star should be bright and close to the target of interest. However, often both criteria cannot be met as the probability of finding a very bright comparison star close to the target is small.

A technique to allow much fainter comparison stars has been proposed that relies on the fact that the systematic trends are often low in frequency. Since the time-scales of these variations are often long, the comparison star light curve can be temporally binned in order to improve the SNR of the comparison star before performing the differential photometry. Hence, high precision photometry can still be achieved with faint comparison stars (Hartley & Wilson 2023).

However, the process of performing differential photometry itself can also induce some small-scale systematic effects such as first-order and second-order atmospheric extinction. First-order atmospheric extinction is caused by the non-negligible difference in airmass between the target and comparison star. The differential airmass will change with time, resulting in the addition of a systematic trend to the calibrated light curve (Mann et al. 2011). To minimize this effect, comparison stars close to the target of interest should be chosen. Second-order extinction is an additional, smaller source of systematic noise, caused by the difference in the spectral energy distribution over the pass-band between the target star and comparison star (Young et al. 1991). This effect depends on the reddening of the Earth's atmosphere and therefore changes from night to night.

In conclusion, the ideal comparison star should be bright and as close to the target star as possible. Using an LGS superimposed with the target star will meet both of these criteria, enabling very high precision ground-based photometry. The use of an LGS as a photometric ratio star for type Ia supernovae photometric data has been previously explored (Albert et al. 2021a,b).

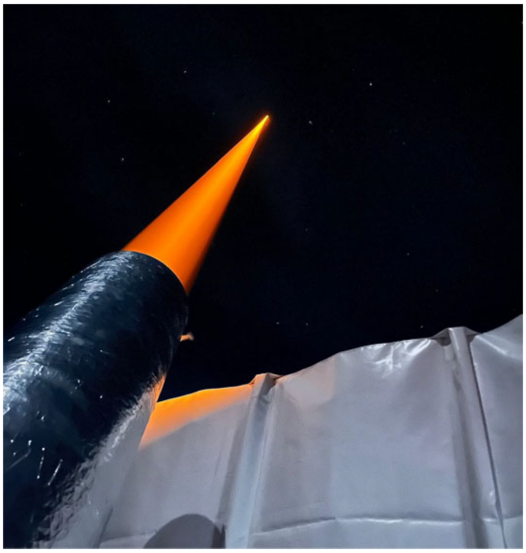

Figure 1. A photo of the 70 W LGS at the Wendelstein LGS unit in La Palma, Canary Islands, Spain.

2.3 Sodium laser guide stars

Sodium laser guide stars (LGS) are artificial reference stars produced by optical excitation of the D2 line in sodium atoms found in the upper mesosphere, using a laser tuned to a wavelength of 589.2 nm. The sodium atoms re-emit the light as they return to the ground state, producing a beacon of light. This layer of sodium atoms in the mesosphere is produced and replenished by the ablation of meteors in the thermosphere. LGSs are useful tools in AO to improve sky coverage when bright natural guide stars are not available (Rigaut & Neichel 2018). The magnitude of the LGS beacon will depend on the power of the laser and the density of the sodium layer. An example of a Sodium LGS is shown in Fig. 1.

However, whilst LGS massively increase the sky coverage for AO, it has several additional error sources. These include the cone effect, spot elongation, and the tip/tilt indetermination problem. Details of these error sources are discussed below.

Since an LGS is at a finite height (~90 km), the light propagates to the telescope aperture through the atmosphere in a cone shape (Tallon & Foy 1990). This means high altitude turbulent layers are sampled by a smaller area than a natural star which can be considered as an infinite distance away. This is shown in Fig. 2. For an LGS, the phase is sampled over a diameter reduced by a factor of:

$$\left(\frac{H_{\rm LGS} - h_j}{H_{\rm LGS}}\right), \tag{4}$$

where $H_{\rm LGS}$ is the altitude of the LGS and h_j is the altitude of the turbulent layer j (Rosensteiner & Ramlau 2013). This difference in sampling causes errors in the measurement of the optical phase aberrations of the incoming wavefronts. This effect is especially bad for large telescopes since the area scales as the square of the aperture size.

The sodium layer is approximately 10 km in thickness. The finite thickness and temporal variations in the density structure of the sodium layer produce elongation, internal structure, and range variations in the LGS beacon (Pfrommer & Hickson 2010). The elongation of the LGS beacon will depend on the thickness of the sodium layer, the distance between the LGS launch, and the receiver telescope and the zenith angle of the target. An example of this is shown in Fig. 3.

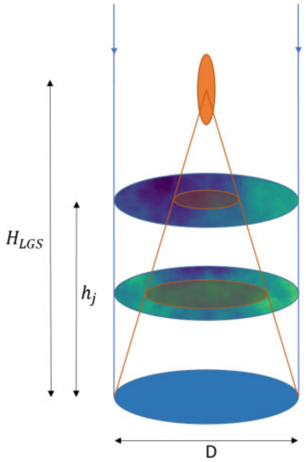

Figure 2. The focal anisoplanatism (cone effect) produced by the finite height of an LGS. This diagram depicts an on axis launch.

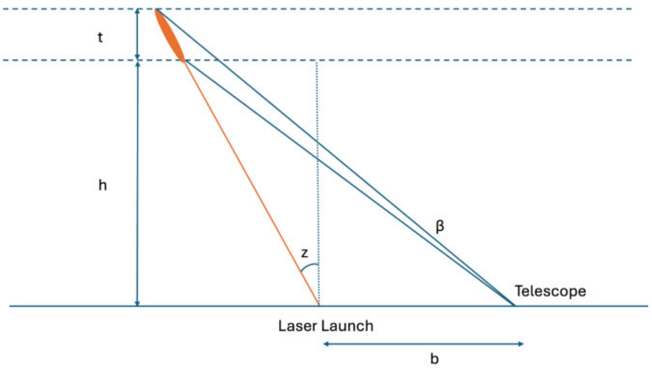

Figure 3. The elongation β of an LGS beacon launched at a zenith angle of z for a separation distance of b between the laser launch and the receiver telescope. This depicts an off axis launch.

The elongation of an LGS beacon is given by the vector $\boldsymbol{\beta} = (\beta_x, \beta_y)$. The magnitude β is the projection of the full-width half-maximums (FWHM) of the sodium profile in the field of view (Tallon & Foy 1990). Hence, the elongation of the LGS beacon is given by (Clare, Louarn & Béchet 2010):

$$\boldsymbol{\beta} = \frac{\cos(z)\boldsymbol{b}t}{h^2}, \tag{5}$$

where z is the zenith angle, $\boldsymbol{b}$ is the baseline vector between the launch telescope and the aperture, t is the thickness of the sodium layer, and h is the mean height of the sodium layer above the telescope.

Another significant problem with using a LGS is that it is impossible to determine the tip/tilt modes of the atmospheric turbulent layers, as the position of the LGS has been affected by the up-link of the laser light as it passes through the atmosphere on its way up to the sodium layer (Pfrommer & Hickson 2010). This is a big problem for AO as ~ 90 per cent of the wavefront error is in tip and tilt (Bonaccini Calia et al. 2014). This problem can be overcome by using a nearby faint NGS to measure the tip and tilt modes since the isoplanatic angle for tip/tilt is often large.

Finally, the atomic density distribution within the sodium layer changes with time, consequently affecting the sodium return flux and its vertical distribution. Sodium altitude fluctuations cannot be distinguished from atmospheric focus changes. Hence, an NGS is required to disentangle these two effects (Rigaut & Neichel 2018).

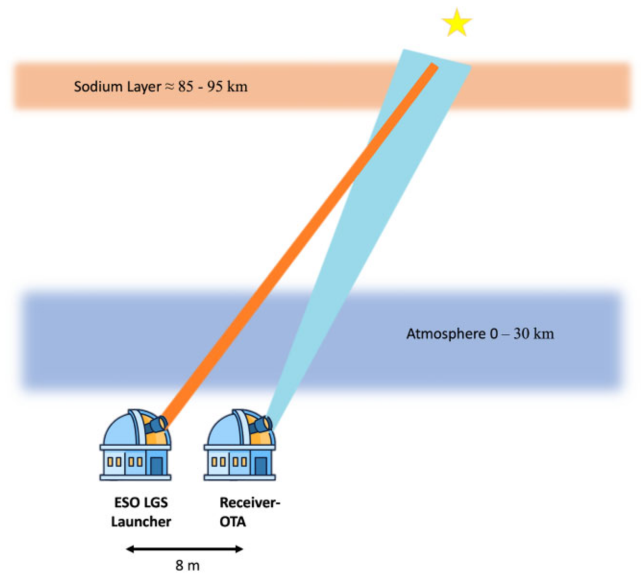

Figure 4. A schematic of the LGS launch telescope with the receiver telescope. The laser beacon excites sodium atoms in the mesosphere producing an artificial LGS beacon directly on top of a target star of interest as viewed from an off axis receiver telescope 8 m from the laser launch. A dichroic filter is used on the receiver telescope to separate the LGS and NGS light sources and re-image them onto a single detector.

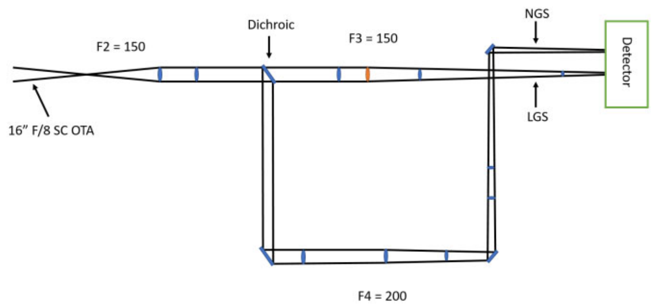

Figure 5. A schematic of the optics used to separate the superimposed NGS and LGS light sources on the receiver telescope. A dichroic beam splitter with transparency at 589.2 nm and a narrow bandpass of 10 nm was used to separate the two light sources. Due to the different optical paths, the NGS has a pixel scale of 0.31 arcsec per pixel and the LGS has a pixel scale of 0.42 arcsec per pixel.

In addition, the sodium laser guide star efficiency is reduced due to spectral hole burning which builds up with increasing laser irradiance. Due to photon recoil, atoms that are initially resonant with the single-frequency laser get Doppler shifted out of resonance, which reduces the pumping efficiency. This effect can be corrected for via the frequency chirping technique (Hellemeier et al. 2022) (Bustos et al. 2020).

In conclusion, sodium LGS are useful tools for astronomers to increase the sky coverage when NGS are not available. However, they have multiple limitations which restrict AO performance. For this technique, the performance will be limited by the cone effect as the LGS will sample smaller areas of the high altitude turbulent layers than the natural target star; by the elongation of the LGS beacon which will lead to averaging of the scintillation noise over the extended source; and finally by variations in the return flux of the laser guide star which will lead to systematic differences between the LGS and the natural target star light curves. The results from an investigation of the impact of the cone effect and laser beacon elongation are presented in Section 4 and suggestions for overcoming the variations in the LGS return flux are presented in Section 5.

3 METHOD

We propose a new technique that uses the light from an LGS to correct scintillation noise and atmospheric transparency variations along a line of sight. An LGS is launched such that the laser beacon is superimposed with a target star of interest as viewed from a neighbouring receiver telescope as demonstrated in Fig. 4.

The light from the two sources can be separated using a narrow-band dichroic beam splitter and either re-imaged on to one detector or onto two separate detectors. Since we are only interested in the intensity of the stars and since we will be using long exposures, any small differences in either the light path length in the one camera case, or small differences in the triggering time for the two camera case, would have negligible effects on the integrated intensity.

Aperture photometry is then performed on the natural star and LGS to produce a light curve for each star. A low order polynomial fit can be used to remove any uncorrelated systematics in the two light curves resulting from the non-common path of the two light sources through the optics system. Differential photometry can then be performed on the natural star light curve using the LGS light curve to remove both scintillation noise and atmospheric transparency variations along the line of sight.

A significant benefit to this scintillation correction technique is that it can be used for any sized telescope. In addition, the technique eliminates first-order atmospheric extinction effects since the LGS starlight and target NGS starlight are passing along the exact same line of sight. However, the performance will be limited by the cone effect of the LGS. In addition, the two light sources may have some remaining non-common systematic noise due to differences in the colour of the star and the LGS as well as any pixel-to-pixel variations on the detector and any field dependent differences on the detector.

A simple experiment to test this method on-sky was performed in May 2024 using the 70 W Wendelstein sodium laser guide star unit at the Roque de los Muchachos observatory, La Palma, Spain. An off-axis Celestron Edge HD14 14 inch receiver telescope which is stationed 8 m from the laser launch telescope was used to collect the target star and the LGS photometric data as demonstrated in Fig. 4. A photo from the laser guide star launch where the LGS has been superimposed with Alioth in Ursa Major is shown in Fig. 1.

The LGS beacon is superimposed with a target star as viewed from the receiver telescope such that the two light sources pass along the same line of sight. An optical system on the receiver telescope that separates the incoming target star light from the laser star light onto a detector was designed and produced by DLR. A dichroic beam splitter with transparency at 589.2 nm and a narrow bandpass of 10 nm is used along with a filter to separate the NGS and LGS light sources. A series of lenses and mirrors are then used to re-image the NGS and LGS onto a single CMOS PCO edge 4 detector as shown in Fig. 5.

The narrow passband and filter ensure that any starlight that leaks through the LGS optical path will be negligible compared to the LGS beacon. Due to the different optical paths, the NGS has a pixel scale of 0.31 arcsec per pixel and the the LGS has a pixel scale of 0.42 arcsec per pixel. The non-common path of the LGS and NGS light through the optics could potentially lead to small systematic errors in the photometric data.

Data packets with a duration of 300 s at a frame rate of 2 Hz were collected. Aperture photometry was performed for the NGS and LGS for each data packet to produce a light curve for each source. To ensure that the LGS was superimposed with the NGS target, only frames where the NGS and LGS were within 1 pixel of the average separation were used. This was to avoid including frames where the wind shake of the laser launch had caused the position of the LGS to shift off the target star. The performance of this technique was compared using the scintillation correction factor, $C_{\rm scint}$, metric which is simply the factor by which the scintillation index has been reduced.

4 RESULTS

In this section we present results from testing this technique in both simulation and on-sky. Error sources including the cone effect and the LGS beacon elongation were explored in simulation. In addition, the correlation angle of the scintillation noise was investigated to determine how close the LGS beacon must be projected to the target star of interest. In all the simulations a 1 s exposure time was used and it has been assumed that the superimposition of the LGS and NGS are perfect. In addition, we have assumed that the LGS intensity is constant with time.

4.1 Cone effect: simulations

The focal anisoplanatism of the LGS will result in a difference between the scintillation noise of the target star photometry and of the LGS photometry. The amount of error due to the cone effect will vary depending on the turbulence profile. The higher the dominant turbulent layers, the more error that will be induced. The maximum scintillation correction that could be achieved will vary significantly due to any variations in the strength of the high layer turbulence. It will also depend on the telescope aperture diameter and will be a more significant error source for larger telescopes.

A simple simulation to estimate the error due to the cone effect for our on sky experimental setup was performed. A single turbulent layer moving at 10 m s^{-1} was simulated for an r_0 of 10 cm using the python package AOTOOLS (Townson et al. 2019). An altitude of 15 km was simulated as a typical height for a strong turbulent layer. A 40 cm telescope observing an LGS at a height of 90 km with an exposure time of 1 s was used. From equation (4), the phase sampled by an LGS at this height will have a radius approximately 16 per cent smaller than the natural target star. It is assumed that the LGS does not have any extent and so only the error due to the cone effect is included.

Fig. 6 shows an example simulated light-curve sequence for a bright star in blue superimposed by an LGS in orange and the calibrated light curve in a green dashed line. The NGS and LGS are strongly correlated in the low frequency intensity fluctuations. On average the scintillation index was reduced by a factor of 8.6 ± 0.4. This shows that whilst the cone effect will limit the correction, significant scintillation noise reduction can still be achieved for the case of a realistic turbulence profile.

For a longer exposure time it is likely that the correction will be higher due to temporal averaging. For long exposure times, the high order spatial scales in the scintillation patterns will average out and the low order spatial scales that are correlated over larger areas are more significant.

4.2 Scintillation correlation angle: simulations

The scintillation correlation angle will depend on multiple parameters including the telescope aperture, the exposure time, wind speed, and wind direction of the high altitude turbulent layers. For large telescopes the scintillation noise will be correlated over much larger angles since there will be a more significant overlap in the high altitude turbulence sampled by both stars. Due to the cone effect, the LGS will likely have a smaller correlation angle with the target star than an NGS would have.

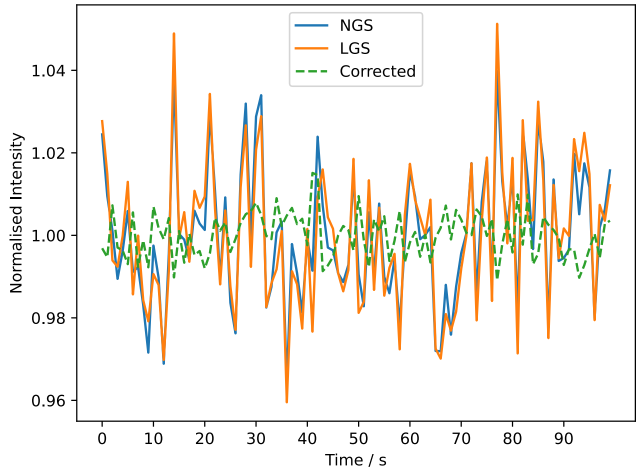

Figure 6. A simulated light curve for a bright star in blue superimposed by an LGS in orange at an altitude of 90 km observed with a 40 cm aperture. The green dashed light curve shows the calibrated star using differential photometry. The difference between the LGS and NGS photometry is purely due to the cone effect.

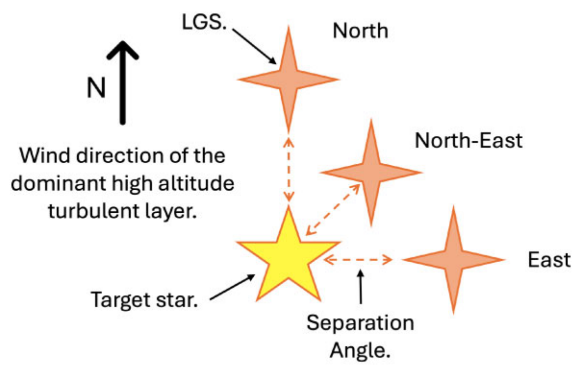

Figure 7. A schematic showing the simulation performed. A single turbulent layer moving North is simulated and the scintillation correction achieved using an LGS separated by varying angles in three directions is measured.

A simple simulation was performed to determine the angle over which scintillation will be correlated for the experiment described. A single turbulent layer at an altitude of 15 km moving at 10 m s^{-1} moving directly North was simulated for an r_0 of 10 cm. A 40 cm telescope observing an LGS at a height of 90 km was used. Taylor's frozen flow hypothesis has been assumed throughout.

Fig. 7 shows a schematic of the simulation performed. A single turbulent layer moving North is simulated and the scintillation correction achieved using an LGS separated by varying angles in three different directions is measured.

Fig. 8 shows the $C_{\rm scint}$ between a star and an LGS on a 40 cm aperture for a range of separation angles and a range of directions. If the LGS is North of the target star (i.e. along the same axis as the turbulent layer wind direction) the scintillation is correlated over large angles due to the time averaging of the scintillation patterns. If however, the LGS is to the East of the star, then the scintillation

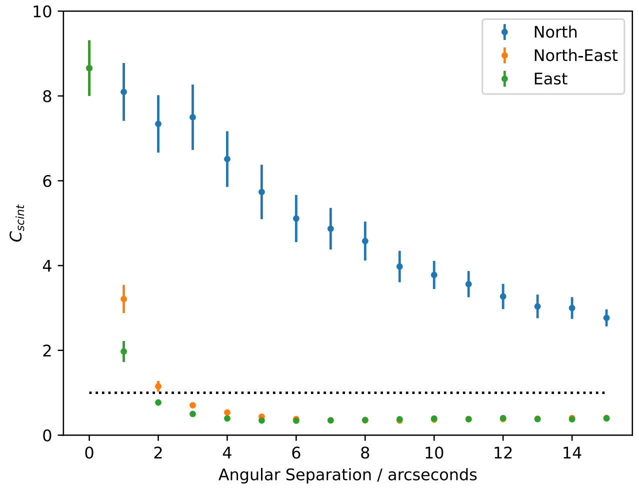

Figure 8. The simulated $C_{\rm scint}$ between a star and an LGS on a 40 cm aperture as a function of the separation angle between the star and LGS for a range of separation directions. The wind direction of the high altitude turbulent layer is North.

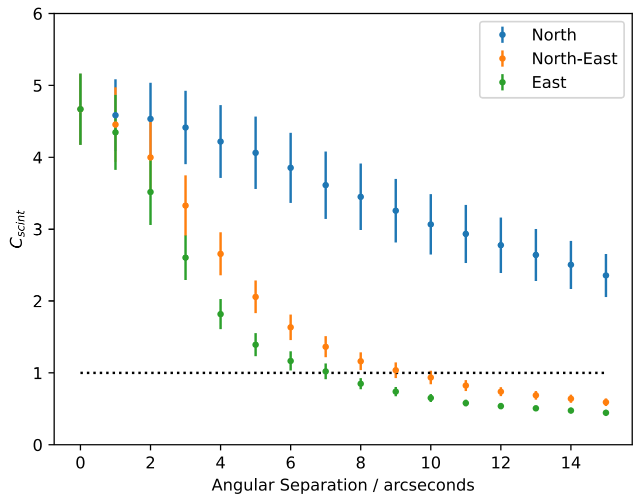

Figure 9. The simulated $C_{\rm scint}$ between a star and an LGS on a 2 m aperture as a function of the separation angle between the star and LGS for a range of separation directions. The wind direction of the high altitude turbulent layer is North.

correlation angle is only $\sim$ 1 arcsec. Similarly, if the LGS is north-east of the target star, the scintillation correlation angle is $\sim$ 2 arcsec. Hence, the LGS would have to be separated from the target star along a direction very close to parallel with the dominant scintillation layer wind direction in order to be correlated over large angles. Hence, for small telescopes, the LGS must be within $\sim$ 2 arcsec in order to provide effective correction of the scintillation noise.

For large telescopes, the scintillation correlation angle will be larger. For example, Fig. 9 shows the same results for a 2 m telescope. In this case, on average the scintillation noise is correlated over a much larger angle of $\sim$ 7 arcsec. However, the error due to the cone effect is more significant meaning that even if the LGS and the target star are completely superimposed, the maximum correction that can be achieved is approximately half that of the 40 cm telescope case.

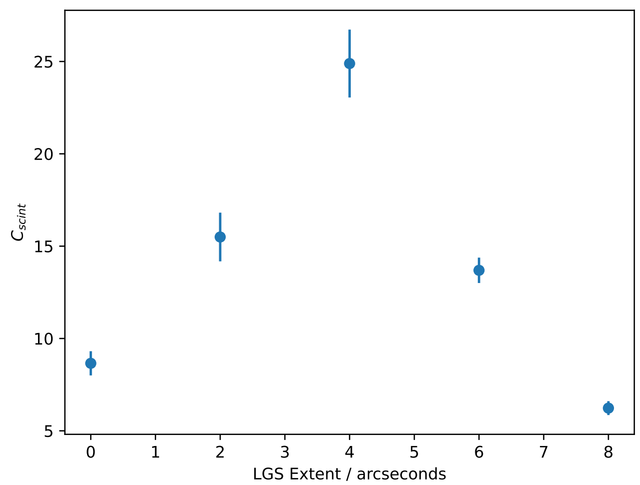

Figure 10. The $C_{\rm scint}$ between a star and an LGS on a 40 cm aperture as a function of the extent of the LGS beacon.

For a longer exposure time it is likely that the correlation angle will be larger due to temporal averaging. However, for a true atmosphere where there will be multiple turbulent layers moving in different directions, the correlation will potentially drop more quickly.

4.3 LGS elongation: simulations

Another error source to consider is the error due to the elongation of the LGS beacon. A simple simulation was performed to determine the effect of the elongated beam on the scintillation correction factor that can be achieved. A single turbulent layer at an altitude of 15 km with wind speed of 10 m s^{-1} moving directly North (0°) was simulated for an r_0 of 10 cm. A 40 cm telescope observing an LGS at a height of 90 km was used. The LGS beacon was elongated by varying amounts and the scintillation correction was recorded. It was assumed that the centre of the elongated LGS was superimposed with the target star and that the intensity of the LGS was constant along the elongated beacon.

Fig. 10 shows the $C_{\rm scint}$ between a star and an LGS on a 40 cm aperture as a function of the extent of the LGS beacon. In this figure, zero extent equates to a point source. For small elongation angles within the scintillation correlation angle, the elongation can actually improve the scintillation correction achieved as the elongation can counter act some of the error due to the cone effect. For large elongation angles, the error due to the inclusion of multiple lines of sight becomes more significant and the scintillation correction decreases. However, we have shown that the elongation of the LGS is not a significant error and can actually improve the scintillation correction performance.

4.4 Zenith angle: simulations

Another important parameter to consider is how the performance varies with the zenith angle. At higher zenith angles the scintillation noise is more significant as the propagation distance to the turbulent layer is increased. The cone effect is independent of zenith angle as both the LGS beacon altitude and the turbulent layer altitude scale equally.

Fig. 11 shows the $C_{\rm scint}$ against zenith angle recorded for the same simulation parameters in Section 4.1. The correction factor increases with zenith angle due to the increased scintillation noise.

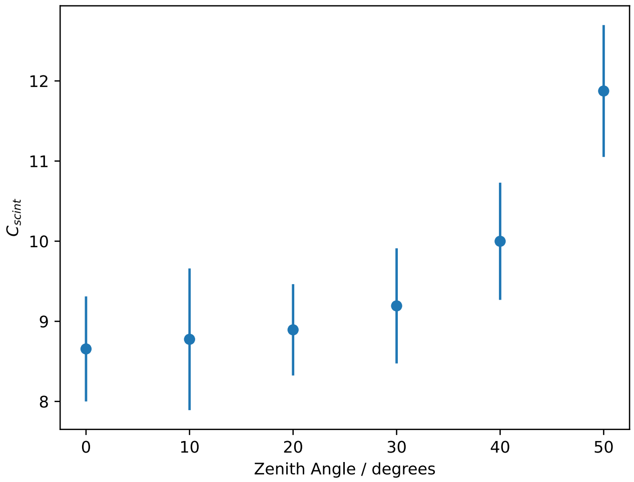

Figure 11. The simulated $C_{\rm scint}$ between a star and an LGS on a 40 cm aperture as a function of the zenith angle. The wind direction of the high altitude turbulent layer is North.

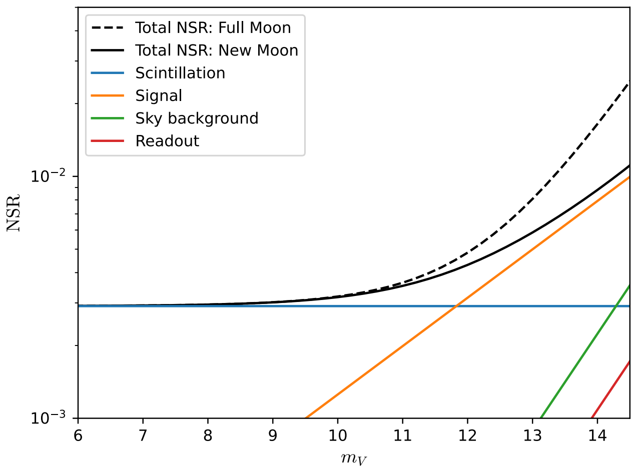

Figure 12. The expected photometric noise contributions based on the CCD equation for the PCO Edge detector on a 14 arcsec telescope observing a *V*-band star with an exposure time of 10 s under typical atmospheric conditions in La Palma. The total noise is plotted for both full moon and new moon.

This suggests that the technique is more beneficial for observations subject to strong scintillation noise.

4.5 On sky experiment

A proof-of-concept experiment was performed in May 2024. Data packets 300 s in length with a frame rate of 2 Hz were collected. Only three data packets were obtained in which the LGS was sufficiently superimposed with the target star. Aperture photometry was performed for the NGS and LGS for each data packet to produce a light curve. The measured seeing for these packets was 0.5 arcsec.

We present the results from testing this method on the 2024 May 19 using two bright stars, HD180530 an A2 type (bluer) star, and HD89332 a K0 type (redder) star, with magnitude 8.9 and 8.7 in the *V* band, respectively, as a target. The 70 W laser produces an ~ 6.6 *V*-band magnitude LGS beacon. Based on Fig. 12, which shows the expected photometric noise contributions for the instrument under typical atmospheric conditions in La Palma, the LGS and natural star photometric noise will be dominated by scintillation. The expected atmospheric transparency variations is hard to estimate, however based on the power spectrum measurements from Hill et al. (1994) at Tiede, the RMS error for our observations would typically be on the order of 5.5×10^{-3}.

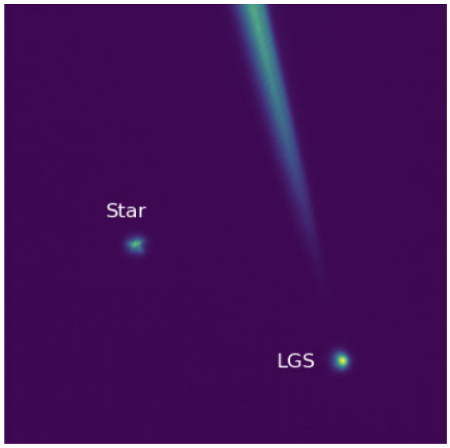

Figure 13. An example typical image frame from the PCO detector showing the star and LGS separated on the detector. Due to the different optical paths, the NGS has a pixel scale of 0.31 arcsec per pixel and the LGS has a pixel scale of 0.42 arcsec per pixel. The LGS plume can be clearly seen in the top right of the image.

Table 1. The scintillation correction measured for each data packet.

Data packet	Frames	$C_{\rm scint}$
HD180530 Packet 1	600 2 Hz	1.70
HD180530 Packet 2	600 2 Hz	4.13
HD89332 Packet 1	500 2 Hz	2.68

Fig. 13 shows an example of a typical image frame from the PCO camera with the star and LGS separated on the detector. The LGS plume can be clearly seen in the top right of the frame. The star is speckled and spread over many pixels therefore significantly increasing the read noise in the measured light curve.

Table 1 shows the scintillation correction factor for three data packets observing either HD180530 or HD89332, which have been temporally binned into 10 s exposures. On average the light-curve variance has been reduced by a factor of 2.8 ± 0.6. The results from this experiment prove the concept and show strong potential for this technique.

Fig. 14 shows the light curves from the HD180530 Packet 2 data packet where the normalized intensity of the NGS is in blue and the LGS in orange. The intensities have been temporally binned into 10 s intervals to maximize the correction achieved, to remove some of the shot and readout noise of both stars and to simulate the expected performance for exposures on the order used in exoplanet transit photometry. A low-order polynomial fit was performed to remove any non-common field-dependent low-order intensity fluctuations on both the NGS and the LGS photometry due to the non-common optical path taken by the two in the instrument optics. The low frequency LGS intensity fluctuations closely match the NGS intensity fluctuations. However, some random high frequency noise still remains. The measured correlation coefficient between the LGS light curve and NGS light curve for this data packet is 0.93. Dividing the

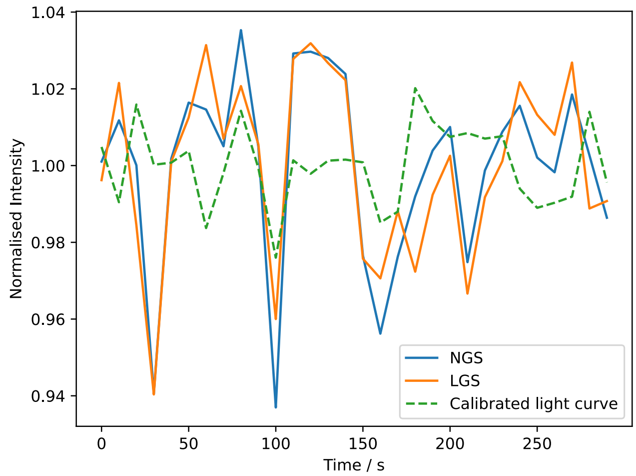

Figure 14. An example data packet of the measured normalized intensity for the NGS in blue and the LGS in orange with the calibrated light curve in green.

NGS light curve by the LGS light curve results in a reduction in the RMS noise in the NGS light curve by a factor of 2.35.

It should be noted that we cannot determine the relative noise contributions from scintillation and from atmospheric transparency variations in the photometric data. Hence, future campaigns should include simultaneous turbulence profile observations to determine the expected scintillation noise and the maximum correction that could be expected based on the cone effect and the LGS beacon elongation. In addition, it is likely there will also be some small random photometric noise contributions such as shot noise and readout noise as well as systematic noise present which will reduce the performance achieved. The results are significantly limited by the guiding and any wind-shake of the LGS beacon. It is expected that improving the stability of the superimposition of the LGS with the NGS would improve the correction achieved.

5 DISCUSSION

We have demonstrated a new technique that uses the light from an LGS to correct for scintillation noise and atmospheric transparency variations. A key benefit of this technique over other scintillation correction techniques such as using tomographic wavefront sensing, is that it requires one single LGS and it can be used on small telescopes.

Another significant benefit of using a superimposed LGS as a comparison star is that it mitigates the first-order extinction effects that occur when using natural comparison stars. However, second-order extinction effects due to the difference in colour between the LGS and the natural star will still occur. This source of noise is usually much smaller than the first-order extinction. The amplitude of the atmospheric transparency fluctuations depends on the size of the absorption features (Mann et al. 2011). Hence, it is possible there will be a small difference between the fluctuations measured in the NGS passband and the LGS passband. A dedicated investigation on the magnitude of this error source over a range of photometric conditions is required.

We have demonstrated that for a small telescope, the scintillation correlation angle is small. Hence, for small telescopes the LGS must be within ~ 2 arcsec of the target star in order to correct the scintillation noise. A significant challenge with this technique however is keeping the LGS and the target star within this small angle, as wind shake of the LGS launch telescope moves it off target. Hence this technique requires very good tracking. As such, it is expected that better performance of this technique could be achieved on a larger telescope where the scintillation correlation angle is larger or by implementing real-time active optics on the laser launch. However, the error due to the cone effect for a large telescope will be more significant. Hence, a trade-off between the cone effect error and the scintillation correlation angle is required and an optimal telescope diameter will exist. In addition, the photometric conditions were very good, and with a seeing of 0.5 arcsec. It is expected that in worse conditions, a higher correction factor could be achieved.

In addition, it is possible that the NGS and LGS will experience different instrumental systematic trends as the two light sources pass through different optical paths and are directed onto different parts of the detector. This would lead to a small systematic error between the photometry for the LGS and the star. Using a flat field could reduce this error. In addition, a simplified instrument that re-images the two light sources onto two detectors may also reduce this error source.

The correction achieved will also depend on the exposure time used with long exposure times resulting in higher correction due to temporal averaging. Exposure times can be increased with the use of diffusers which have the additional benefit of reducing systematic noise due to pixel-to-pixel variations (Stefansson et al. 2017).

An important error source that we have not yet discussed is the variation of the LGS return flux with time due to changes in the sodium layer density. This will lead to a systematic error in the LGS intensity which cannot be distinguished from the atmospheric induced intensity variations in the photometric data. This error is unlikely to be significant for our observations as we have only observed short time-scales. However, it would be a problem on the time-scales of exoplanet transit observations. Hence, to compensate for this error, the variations of sodium layer would need to be monitored using a LiDAR or an off-axis telescope. The expected return flux (Holzlohner et al. 2010) based on these measurements can then be used to calibrate the LGS signal.

Alternatively, if this is not available, differential photometry of the LGS light curve with a nearby faint comparison star could be used with temporal binning to isolate the low order LGS intensity fluctuations due to the varying sodium layer from the fluctuations due to the atmosphere. A low order fit of the calibrated LGS light curve can then be used to estimate the LGS return flux variations which can then be used to calibrate the raw LGS light curve.

6 CONCLUSIONS

We have presented a new technique capable of providing very high precision ground-based photometry. An LGS is superimposed directly on top of a target star of interest as viewed from a receiver telescope such that the two light sources pass along the exact same line of sight. The light sources are separated using a dichroic beam splitter and the LGS photometry is used to calibrate the target star light curve.

A proof-of-concept experiment was performed in May 2024 using the Wendelstein LGS Unit in La Palma, Spain. Results from this experiment showed that the variance of the target star was reduced by a factor of 2.8 ± 0.6 on average. These results were limited by the unstable superimposition of the LGS beacon with the target star and it is expected that improving the stability would lead to significant gains in performance. Future experiments to test this technique on a wider variety of turbulence profiles and atmospheric conditions are required. In addition, this technique needs to be tested on a target of interest such as an exoplanet transit where variations in the LGS return flux must also be accounted for.

ACKNOWLEDGEMENTS

The reported observations were carried out in the frame of ESO Laser Guide Star Systems R&D activities. We would like to thank Ramon Mata Calvo and Ricardo Barrios for the OTA and the optical system developed at DLR.

KH and JO acknowledge support from UK Research and Innovation (Future Leaders Fellowship MR/X015106/1).

This research made use of Python including NUMPY and SCIPY (van der Walt, Colbert & Varoquaux 2011), MATPLOTLIB (Hunter 2007), ASTROPY, a community-developed core Python package for Astronomy (The Astropy Collaboration 2013), the Python AO utility library AOtools (Townson et al. 2019).

DATA AVAILABILITY

Please contact the lead author for data availability.

REFERENCES

Albert J. E., Budker D., Chance K., Gordon I. E., Pedreros Bustos F., Pospelov M., Rochester S. M., Sadeghpour H. R., 2021a, MNRAS, 508, 4399

Albert J. E., Budker D., Chance K., Gordon I. E., Bustos F. P., Pospelov M., Rochester S. M., Sadeghpour H. R., 2021b, MNRAS, 508, 4412

Bonaccini Calia D., Hackenberg W., Holzlöhner R., Lewis S., Pfrommer T., 2014, Adv. Opt. Technol., 3, 345

Bonnacini Calia D. et al., 2012, in Navarro R., Cunningham C. R., Prieto E., eds, Proc. SPIE Conf. Ser. Vol. 8450, Modern Technologies in Space- and Ground-based Telescopes and Instrumentation II. SPIE, Bellingham, p. 84501R

Bustos F. P., Holzlöhner R., Rochester S., Calia D. B., Hellemeier J., Budker D., 2020, J. Opt. Soc. Am. B, 37, 1208

Clare R. M., Louarn M. L., Béchet C., 2010, Appl. Opt., 49, G27

Collins K. A. et al., 2018, AJ, 156, 234

Dravins D., Lindegren L., Mezey E., Young A. T., 1997, PASP, 109, 173

Föhring D., Wilson R. W., Osborn J., Dhillon V. S., 2019, MNRAS, 489, 5098

Hartley K. E., Wilson R. W., 2023, MNRAS, 526, 3482

Hartley K. E., Farley O. J. D., Townson M. J., Osborn J., Wilson R. W., 2023, MNRAS, 520, 4134

Hellemeier J. et al., 2022, MNRAS, 511, 4660

Hill F. et al., 1994, Sol. Phys., 152, 321

Holzlohner R., Rochester S., Pfrommer T., Calia D., Budker D., Higbie J., Hackenberg W., 2010, in Ellerbroek B. L., Hart M., Hubin N., Wizinowich P. L., eds, Proc. SPIE Conf. Ser. Vol. 7736, Adaptive Optics Systems II. SPIE, Bellingham, p. 77360V

Howell S. B., 2006, Handbook of CCD Astronomy, 2 edn. Cambridge Observing Handbooks for Research Astronomers. Cambridge Univ. Press, Cambridge

Hunter J. D., 2007, Comput. Sci. Eng., 9, 90

Kornilov V., 2012, MNRAS, 426, 647

Mann A. W., Gaidos E., Aldering G., 2011, PASP, 123, 1273

Osborn J., 2014, MNRAS, 446, 1305

Osborn J., Wilson R., Butterley T., Shepherd H., Sarazin M., 2010, MNRAS, 406, 1405

Osborn J., Föhring D., Dhillon V. S., Wilson R. W., 2015, MNRAS, 452, 1707

Pfrommer T., Hickson P., 2010, in Ellerbroek B. L., Hart M., Hubin N., Wizinowich P. L., eds, Proc. SPIE Conf. Ser. Vol. 7736, Adaptive Optics Systems II. SPIE, Bellingham, p. 773620

Pont F., Zucker S., Queloz D., 2006, MNRAS, 373, 231

Rigaut F., Neichel B., 2018, ARA&A, 56, 277

Roddier F., 1981, in Wolf E., ed., Progress in Optics, Vol. 19, V The Effects of Atmospheric Turbulence in Optical Astronomy. Elsevier, Amsterdam, Netherlands, p. 281

Rosensteiner M., Ramlau R., 2013, J. Opt. Soc. Am. A, 30, 1680

Sasiela R. J., 2012, Electromagnetic Wave Propagation in Turbulence: Evaluation and Application of Mellin Transforms. Springer Series on Wave Phenomena Vol. 18. Springer, Berlin

Stefansson G. et al., 2017, ApJ, 848, 9

Tallon M., Foy R., 1990, A&A, 235, 549

The Astropy Collaboration 2013, A&A, 558, A33

Townson M. J., Farley O. J. D., de Xivry G. O., Osborn J., Reeves A. P., 2019, Opt. Express, 27, 31316

van der Walt S., Colbert S. C., Varoquaux G., 2011, Comput. Sci. Eng., 13, 22

Young A. T. et al., 1991, PASP, 103, 221

Zou H. et al., 2010, AJ, 140, 602

This paper has been typeset from a TEX/LATEX file prepared by the author.